Optical design of interferometric telescopes with wide fields of view

Erin E. Sabatke, James H. Burge, and Philip Hinz

The performance of wide-field multiple-aperture imaging systems is dominated by easily understood, low-order errors. Each aperture produces an individual image, each pair of apertures produces a set of fringes under a diffraction envelope, and the system bandwidth produces a coherence envelope. For wide-field imaging, each of these elements must be coincident in the image plane as the field angle changes. We explore the causes of image degradation, derive first-order rules for preserving image quality across field, and give an example design that enforces some of the rules to achieve a relatively wide-field interferometric imaging telescope.

OCIS codes: 350.1260, 110.6770, 220.2740, 220.1000, 120.3180.

1. Introduction

Telescopes that rely on monolithic primary mirrors can gain in sensitivity and resolution only by increasing the diameter of the primary mirror, which is usually the entrance pupil of the system. The astronomical community is rapidly approaching hard constraints on its ability to continue to produce larger monolithic primaries. Imaging interferometers can sidestep these fabrication constraints and produce high-resolution images over wide fields of view. With the proper choice of a beam combiner, two or more monolithic primaries can operate as a single telescope with a resolution limited only by the mirror separation (baseline) of the system and a sensitivity limited by the combined collection area of the monolithic primary mirrors. The optical design of the beam combiner is critical because the beam combiner ultimately limits the field of view of the system.

Interferometric imaging over wide fields of view has a fairly long history in the literature, though it is only recently that adaptive optics has made the technique practical in the IR and optical regimes. Diffraction modeling of the PSFs and transfer functions began in the late 1960s.[1,2] Some work was done to find the optimal positions for a given number of apertures.[3,4] Meinel was the first to recognize and propose a solution for correcting the linear piston errors in wide-field interferometric systems,[5] while Traub contributed important proofs of the requirements for beam combining.[6] Progress was made on aberration analysis in multiple aperture systems.[7,8] Distortion problems have been investigated in specific systems.[9,10] Field-of-view limitations and general design principles have also been discussed.[11–16] This paper will add to that body of work by providing practical guidelines for the design of beam combiners and a clear conceptual understanding of beam-combining errors.

The first telescope to succeed in wide-field interferometric imaging for short periods of time was the Multiple Mirror Telescope (MMT) near Tucson, Arizona.[17] The technological successor of the MMT is the Large Binocular Telescope (LBT) currently being built on Mount Graham in Arizona. The LBT will be the first telescope that can operate full-time in the wide-field interferometric mode.[18] The telescope uses two primaries, each with a diameter of 8.2 m, on a baseline of 14.4 m. Each primary is a symmetric, on-axis mirror; the two mirrors are not off-axis pieces of a larger parent prescription. A schematic of the optical layout is shown in Fig. 1, including an enlarged view of a beam combiner designed by Phil Hinz. Each arm of the beam combiner consists of two fold flats and an off-axis ellipse and produces a beam at $f/41.3$. Combining the two $f/41.3$ beams results in a faster system at $f/15$ with a 1 arcmin field of view.

The LBT beam combiner design will be used as an example throughout this paper. We first examine the

E. Sabatke (esabatke@ball.com) and J. Burge (jburge@optics.arizona.edu) are with the Optical Sciences Center, University of Arizona, 1630 East University Boulevard, Tucson, Arizona 85721-0094. P. Hinz (phinz@as.arizona.edu) is with the Steward Observatory, University of Arizona, 922 North Cherry Avenue, Tucson, Arizona 85721-0065.

Received 8 March 2006; revised 27 June 2006; accepted 28 June 2006; posted 3 July 2006 (Doc. ID 68739).

0003-6935/06/318026-10$15.00/0

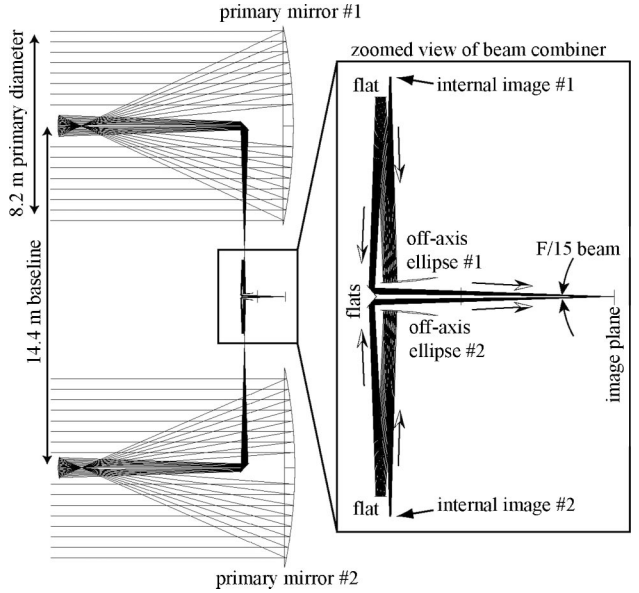

Fig. 1. Optical schematic of the LBT, including an enlarged view of the beam combiner.

perfect image from a LBT-like system. We find that the image consists of four components: an image from each of the two apertures, a set of fringes, and a coherence envelope. These components need to be collocated on the image plane as a function of field to achieve a wide-field image of the required fidelity. Errors in the image are then discussed one at a time: shift of the fringes is due to piston errors between apertures, lateral image separation is caused by relative tilt between the two apertures, and longitudinal image separation is caused by defocus errors between the apertures. We discuss how each of these errors can be corrected while the system's beam combiner is being designed.

Constructing a nonsequential (NSQ) model of these systems can be difficult and time consuming. Optimization of such a nonsequential model is also difficult. However, an understanding of beam-combining errors allows one to complete most of the design by modeling only one arm of the system in a sequential setup. This allows one to make better use of design and optimization tools that are built into the major ray-trace codes.

2. The Perfect Image

The perfect image from a two-aperture telescope such as the LBT has simple parts that can be calculated analytically. Let the apertures be circular with diameters D_1 and D_2 and the aperture centers be located at (x_1, y_1) and (x_2, y_2). The apertures are uniformly illuminated with an intensity of 1. The amplitude function of the system is

$$A(x, y) = \mathrm{Cyl}\left(\frac{1}{D_1}[(x - x_1)^2 + (y - y_1)^2]^{1/2}\right) + \mathrm{Cyl}\left(\frac{1}{D_2}[(x - x_2)^2 + (y - y_2)^2]^{1/2}\right), \quad (1)$$

where

$$\mathrm{Cyl}(r) = \begin{cases} 1 & r < 1/2 \\ 0 & r > 1/2 \end{cases}.$$

For an on-axis point source at infinity, the monochromatic intensity of a combined image from the two-aperture system is related to the Fourier transform of Eq. (1):

$$I(x, y) = \left(\frac{1}{\lambda f}\right)^2 \left\{ \left(\frac{\pi D_1^2}{4}\right)^2 \mathrm{Somb}^2\left(\frac{D_1}{\lambda f} r\right) + \left(\frac{\pi D_2^2}{4}\right)^2 \mathrm{Somb}^2\left(\frac{D_2}{\lambda f} r\right) + 2\left(\frac{\pi D_1 D_2}{4}\right)^2 \mathrm{Somb}\left(\frac{D_1}{\lambda f} r\right) \mathrm{Somb}\left(\frac{D_2}{\lambda f} r\right) \times \cos\left[\frac{2\pi}{\lambda f}(x_1 - x_2)x + \frac{2\pi}{\lambda f}(y_1 - y_2)y\right] \right\}, \quad (2)$$

where the function $\mathrm{Somb}(\rho) = [2J_1(\pi\rho)]/(\pi\rho)$ and J_1 is the first-order Bessel function of the first kind.[19] The focal length of the combined telescope is f, λ is the wavelength, and $r = (x^2 + y^2)^{1/2}$ as measured in the pupil. If $D_1 = D_2 = D$ and the baseline has a length of Δ and is collinear with the x axis, then Eqs. (1) and (2) simplify to

$$A(x, y) = \mathrm{Cyl}\left(\frac{1}{D}\left[\left(x - \frac{\Delta}{2}\right)^2 + y^2\right]^{1/2}\right) + \mathrm{Cyl}\left(\frac{1}{D}\left[\left(x + \frac{\Delta}{2}\right)^2 + y^2\right]^{1/2}\right), \quad (3)$$

$$I(x, y) = \left(\frac{\pi D^2}{2\lambda f}\right)^2 \mathrm{Somb}^2\left(\frac{D}{\lambda f} r\right) \cos^2\left(\frac{2\pi}{\lambda f}\frac{\Delta}{2} x\right). \quad (4)$$

A plot of the point spread function (PSF) generated from Eq. (4) is shown in Fig. 2 for the case of large apertures on a relatively short baseline.

A. Errors that Can Degrade the Perfect Image

The image described by Eq. (2) is the sum of three parts: an image from the first aperture, an image from the second aperture, and a set of cosine fringes under an envelope. Keeping this picture in mind, there are only three kinds of error that can degrade the image:

1. Images shift apart: the individual images separate from one another in any direction.
2. Fringes shift away from the images: the peak of the fringes move away from the individual aperture's images.
3. Aberrations: the individual images are aberrated.

A conceptual sketch of the beam-combining errors is shown in Fig. 3.

These errors are not unique to two-aperture systems. The image of a three-aperture system, for example, will contain three images from the individual apertures and three sets of cosine fringes (one set of

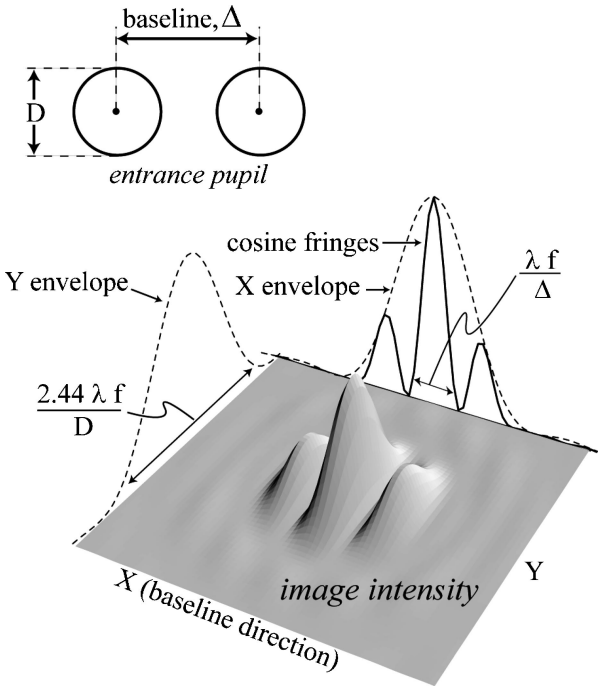

Fig. 2. Entrance pupil and PSF for a two-aperture system with large apertures on a relatively short baseline.

fringes for each aperture pair, each oriented perpendicularly to the baseline between the two apertures). The perfect image in the three-aperture case has the same possible errors: the images can move apart, any of the fringe sets can move away from the center, and any of the individual images can be aberrated.

B. Appearance of the Errors in Wave Fans

Each of the beam-combining errors will appear in the wave fans of a multiple-aperture system. (Wave fans here refers to plots of the optical path difference versus the pupil coordinate.) A shift of the fringes appears as a piston error between the apertures, lateral shift of an image appears as a tip or tilt error between apertures, and axial shift of an image appears as a power error across an aperture. Higher-order aberrations appear in the usual way. Figure 4 shows wave fans from a nonsequential model of a three-aperture system whose beam combiner has not been corrected for beam-combining errors. The three apertures are circular, equal in diameter, and in a line such that the edges of the apertures touch. The low-order design errors in the beam combiner dominate the degradation in the system's performance. Power, tilt, and piston errors appear with increasing field angles [see Figs. 4(b) and 4(c)]. Such wave fans can be easily reconstructed by using a ray-trace model of a single arm of a system; a full nonsequential model is not required for predicting these wave fans.

3. Piston Errors between Apertures Cause a Shift of the Fringe Center

A. Effect of Piston Errors on the Perfect Image

Piston errors cause the fringe center to move away from the combined subimages. This can be shown analytically. With a piston error of δ waves between the two apertures, Eq. (3) becomes

$$A(x, y) = \mathrm{Cyl}\left(\frac{1}{D}\left[\left(x - \frac{\Delta}{2}\right)^2 + y^2\right]^{1/2}\right) + \exp(i\pi\delta)\mathrm{Cyl}\left(\frac{1}{D}\left[\left(x + \frac{\Delta}{2}\right)^2 + y^2\right]^{1/2}\right). \quad (5)$$

The monochromatic PSF from the system becomes

$$I(x, y) = \left(\frac{\pi D^2}{4\lambda f}\right)^2 \mathrm{Somb}^2\left(\frac{D}{\lambda f} r\right) + \left(\frac{\pi D^2}{4\lambda f}\right)^2 \mathrm{Somb}^2\left(\frac{D}{\lambda f} r\right) + 2\left(\frac{\pi D^2}{4\lambda f}\right)^2 \mathrm{Somb}^2\left(\frac{D}{\lambda f} r\right)\cos\left(\frac{2\pi\Delta}{\lambda f} x + \pi\delta\right). \quad (6)$$

The effect of the piston error (δ) is a shift of the cosine fringes. Note that the Somb envelope over the fringes in the third term on the right-hand side of Eq. (6) is tied to the individual images and does not shift. As the cosine fringes shift, their peak is reduced in height as it follows the height of the Somb envelope. The height of the total PSF is reduced.

An example of the effect is shown in Fig. 5. PSFs from Eq. (6) were generated for two apertures, each 1 m in diameter. The wavelength (λ) is 0.5 μm, the system focal length (f) is 10 m, and the baseline (Δ) is

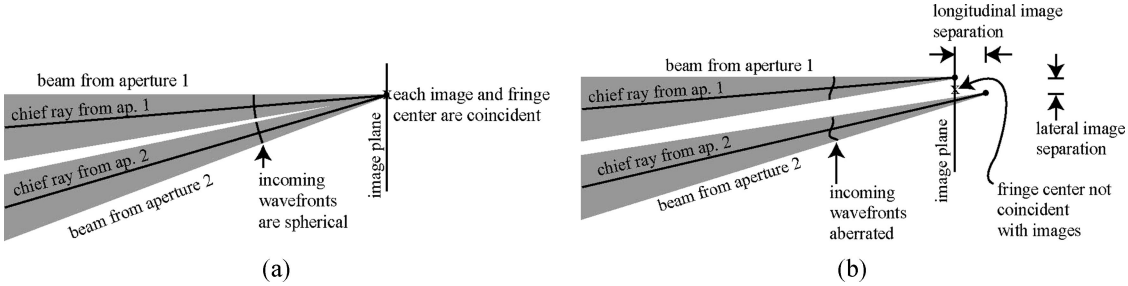

Fig. 3. (a) For perfect beam combining, the images from each aperture and the fringe center must be coincident in the image plane of the system. (b) The only errors that can occur during beam combining are lateral and longitudinal separation of the images, fringes that shift away from the images, and aberrated wavefronts in any of the subapertures of the system.

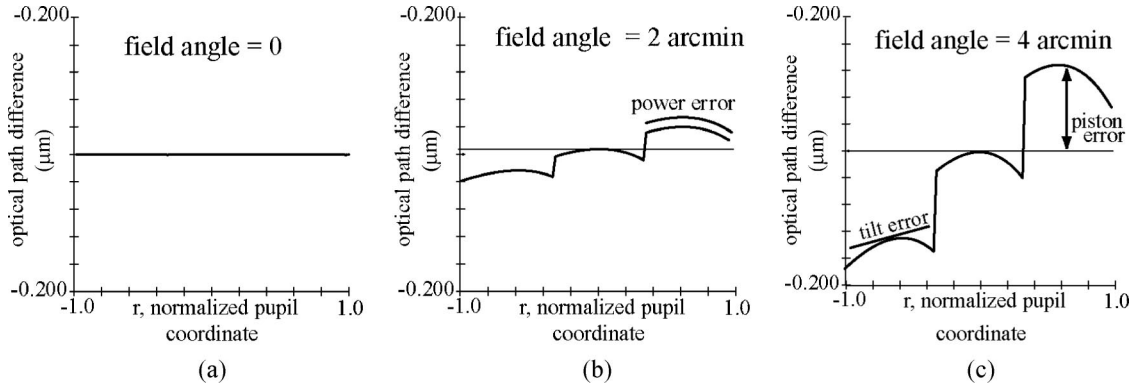

Fig. 4. (a) On-axis wave fan for a three-aperture imaging interferometer whose beam combiner has not been corrected for low-order beam combining errors. (b), (c) Wave fans for an imaging interferometer whose beam combiner has not been corrected for low-order beam combining errors show power, tilt, and piston errors at (b) a 2 arcmin and (c) a 4 arcmin field angle.

1.5 m. Piston errors (δ) of 0, 0.15, and 0.4 waves are shown in Figs. 5(a), 5(b), and 5(c).

B. Polychromatic Point Spread Function

The polychromatic PSF is just the monochromatic PSF integrated over the bandwidth, and this introduces a coherence envelope to the cosine fringes. The width of the coherence envelope is set by the spectrum's bandwidth and multiplies with the Somb envelope already over the fringes.

In the monochromatic case shown in Fig. 5, the Strehl ratio will return to 1 every time the piston error reaches an integer number of waves so that a cosine fringe is aligned with the center of the envelope function. The coherence function in the monochromatic case is infinitely wide and does not affect the PSF height. The height of the more realistic polychromatic PSF, though, will continue to fall with increasing piston error due to the coherence envelope over the fringes. The monochromatic and polychromatic Strehl heights are plotted in Fig. 6.

If the bandwidth is narrow and the system has large apertures on relatively short baselines, the Somb envelope will dominate the degradation of the PSF for piston errors less than π (see Fig. 6). If the bandwidth is wide, though, the coherence envelope will be quite narrow and may be the initial limitation on the field of view. Systems with small apertures on long baselines have wide Somb envelopes; the fields of view of such systems will be limited by the coherence envelope, which allows very wide fields of view for narrow bandwidths. These systems have broad PSFs that do not allow direct imaging, however.

Figure 7 shows a series of polychromatic PSFs as the piston error increases. The calculations were done for a two-aperture system with a baseline of 14.4 m and aperture diameters of 8.4 m. The rectangular spectrum was centered on $\lambda = 4.8$ μm and had a width of 1.2 μm for a coherence length of roughly 16 μm. (One estimate of coherence length is $l_c = c/\Delta\nu$, where c is the speed of light and $\Delta\nu$ is the frequency bandwidth.) At about twice the coherence length, the interference between the two beams is completely gone because the fringes have shifted out from under the Somb envelope; the portion of the fringes now centered under the Somb envelope has almost no modulation because of suppression by the coherence envelope. The telescope is operating in a light-bucket mode; it has better sensitivity than a single aperture but no better resolution.

C. Evaluating Piston Errors in a Ray-Trace Model

Ray-trace data can be used to create an estimate of the combined wave fan such as those in Fig. 4. A chief ray (a ray from a given field angle and passing

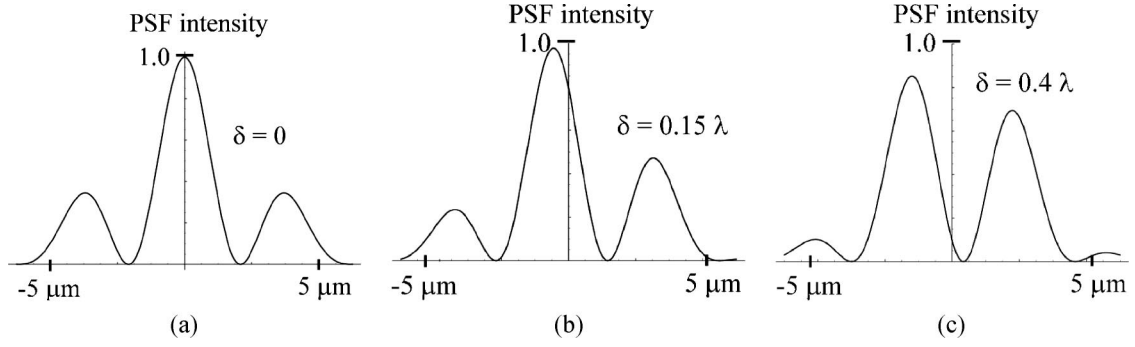

Fig. 5. Cross sections of the monochromatic PSF from a two-aperture system with piston errors of (a) $\delta = 0$ waves, (b) $\delta = 0.15$ waves, (c) $\delta = 0.4$ waves. For Eq. (6) $D = 1$ m, $\lambda = 0.5$ μm, $f = 10$ m, and $\Delta = 1.5$ m.

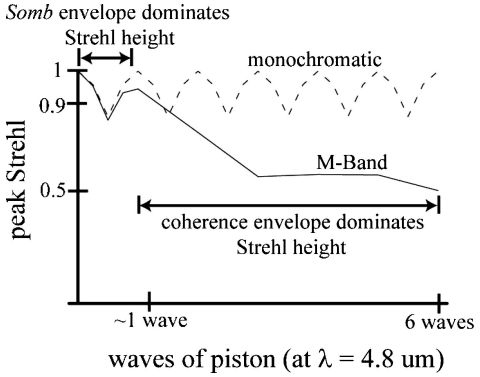

Fig. 6. Monochromatic PSF recovers every time the piston passes through π, so that a cosine fringe is centered under the Somb envelope, but the more realistic polychromatic PSF continues to degrade because of the addition of the coherence envelope.

through the center of the primary or entrance pupil) must be traced in each arm of the system. The optical path length (OPL) of each ray should be calculated, and the difference between the chief ray OPLs divided by the operational wavelength (ΔOPL/λ) gives the piston in waves.

D. Eliminating Constant Piston Errors by Matching On-Axis Path Lengths

Piston errors that are constant as a function of field angle are caused by a mismatch in the axial path lengths of each arm of the interferometer. A ray trace of the on-axis chief rays (axial rays) for each arm in the system will show mismatched OPLs between the entrance pupil and the image plane of the system. If the arms of the interferometer are identical and equidistant from the system image plane, this error cannot occur.

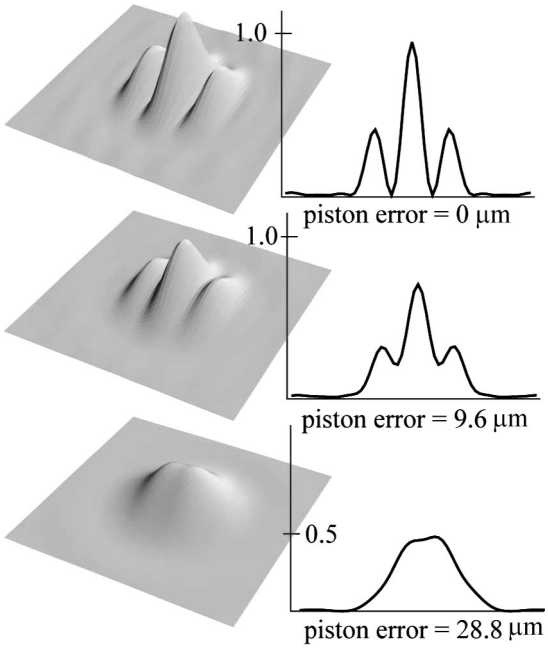

Fig. 7. PSFs of a two-aperture system with increasing piston errors. The system consisted of two 8 m apertures on a 14 m baseline. The center wavelength was 4.8 μm with a bandwidth of 1.2 μm.

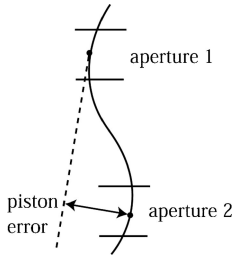

Fig. 8. Linear piston errors in a multiple-aperture system can be viewed as coma in the parent system and can be eliminated by satisfying the Abbe sine condition for the axial rays in each arm of the interferometer.

E. Eliminating Linear Piston Errors by Satisfying the Abbe Sine Condition

For a system that is not corrected for beam-combining errors, the difference between the OPLs for two arms of the interferometer will generally differ as a linear function of field angle. Figure 4 shows the wavefronts in such a situation.

This linear piston error is related to a coma error in a conventional system. The sketch in Fig. 8 shows that, if the parent system's wavefront contains coma, two segments taken from the parent wavefront will appear to have a relative piston error. Coma varies linearly with field angle, so the piston error is also linear with field angle.

Since coma can be corrected by satisfying the Abbe sine condition,[20] linear piston errors in a multiple aperture system can also be eliminated in this way. For finite conjugates, the Abbe sine condition has the form

$$m = \sin u'/\sin u, \tag{7}$$

where m is the paraxial system magnification, u is the marginal ray angle in object space, and u' is the marginal ray angle in image space. To eliminate coma, Eq. (7) must be satisfied for all u. For infinite conjugates, the height of the marginal ray is substituted for the object space marginal ray angle:

$$h = a \sin u', \tag{8}$$

where h is the height of the marginal ray in the entrance pupil and a is a constant. To eliminate coma, the condition must be satisfied for all h.

This condition has been derived in other forms.[6,21] Equations (7) and (8) can both be interpreted as requiring that the entrance pupil and exit pupil configurations be scaled copies of each other. Both equations can be reduced to the form $h/h' = \kappa$, where κ is a constant and h' is the height of the marginal ray in the exit pupil. The pupil scaling concept is useful

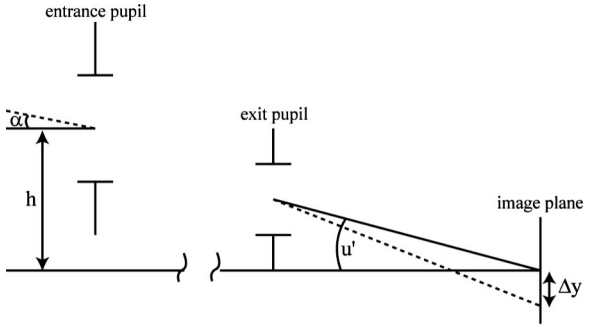

Fig. 9. Parameters used in Eq. (9) to correct linear piston errors.

for the initial design of a multiple-aperture system; none of the beams can be flipped or incorrectly positioned between the entrance pupil and the exit pupil. For optimization in a ray-trace program, though, the marginal rays defining the edges of the apertures in the exit pupil are likely to be aberrated. A more useful form to use in optimization relies on rays that are close to the axial rays:

$$h/\sin u' = \Delta y/\alpha, \tag{9}$$

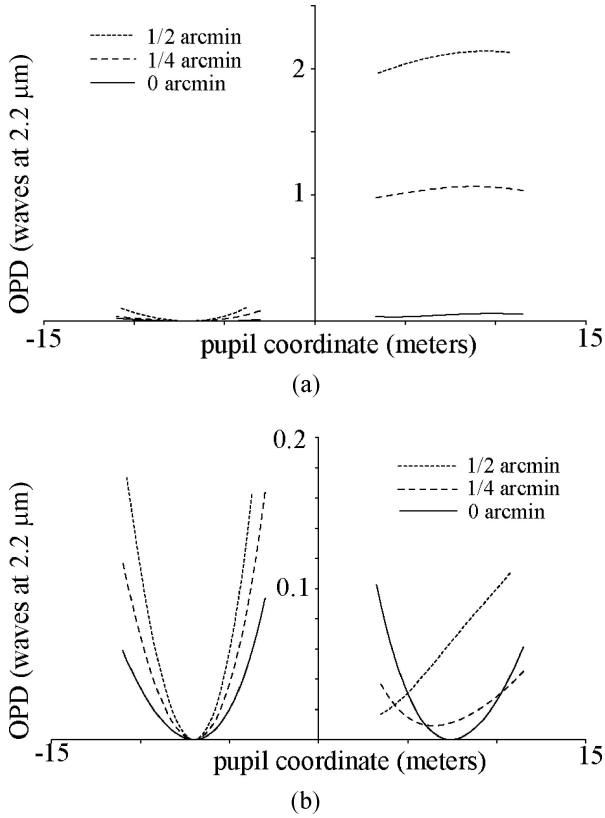

Fig. 10. (a) Wave fans before the sine condition is applied to the LBT beam-combiner design. Field angles of 0, 1/4, and 1/2 arcmin are shown. (b) Wave fans after the sine condition is applied to the LBT beam-combiner design. (Note the 10× scale change between (a) and (b).

where h is again the height of a ray in the entrance pupil at zero field angle, u' is the output angle of the ray in image space, α is a very small field angle for a ray traced at the same height in the image plane, and Δy is the height of that ray in the image plane (see Fig. 9).

Coma can be seen as a change in focal length versus zone in the pupil. Equation (9) can be interpreted as demanding that the focal length ($\Delta y/\alpha$) as a function of zone in the pupil stay constant for small field angles. Technically, to eliminate linear piston errors the condition needs to be satisfied only for the axial ray location in the entrance pupil (h) for each arm of the interferometer.

F. Correction of Linear Piston in the Large Binocular Telescope

A beam combiner designed with only single-arm performance in mind usually results in a system dominated by piston errors that are linear with field angle. Figure 10 shows wave fans from such a blind beam-combiner design for the LBT. The single-arm performance is good, the beam combiner fits in the available space, and the f-number and combined f-number of the beams are correct, but the linear piston error is quite large.

After correction of the linear piston errors by using an optimization based on Eq. (9), the system's performance is improved by a factor of 10. The system is now limited by astigmatism in the individual arms rather than low-order beam-combining errors, as the spot diagrams in Fig. 11(b) show. Some on-axis performance was sacrificed to correct the linear piston errors, with the result that the broadband PSF is coherent over a much larger field of view [compare Figs. 11(a) and 11(b)].

The linear piston error shown in Fig. 10 is evident even in a ray-trace model of a single arm. Because of the geometry of the LBT, a negative Y field angle for the upper arm of the beam combiner is a positive Y field angle for the lower arm of the beam combiner (see Fig. 1). For the linear piston to be zero, the path length of an axial ray through a single arm of the beam combiner should be equal for very small positive and negative Y field angles.

Figure 12 shows the difference in each aperture's axial ray path length as a function of field angle. One set of data was generated by using a model of the single arm; the other set was generated by using a full nonsequential model of the two-aperture system. Both sets of data show that the slope near the center is zero, indicating that the linear piston term has been properly corrected.

4. Tilt Errors between Apertures Cause Lateral Image Separation

A. Effect of Tilt Errors on the Perfect Image

A tilt error in one of the apertures will cause one of the individual Somb^2 images to move away from the remaining images. For a two-aperture system, the amplitude function describing the entrance pupil will be

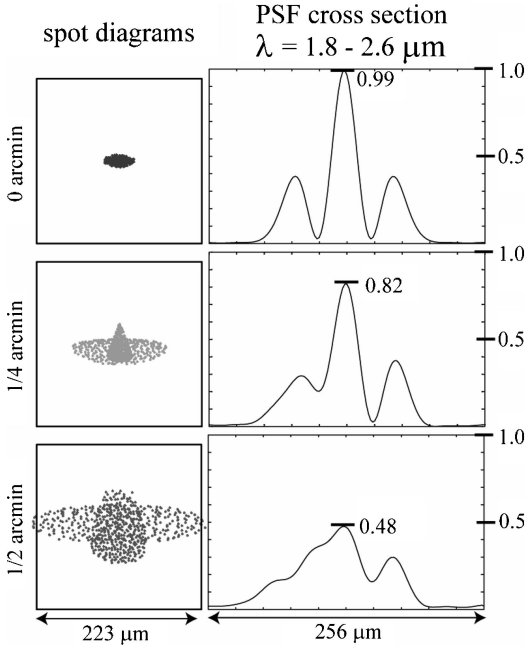

(a)

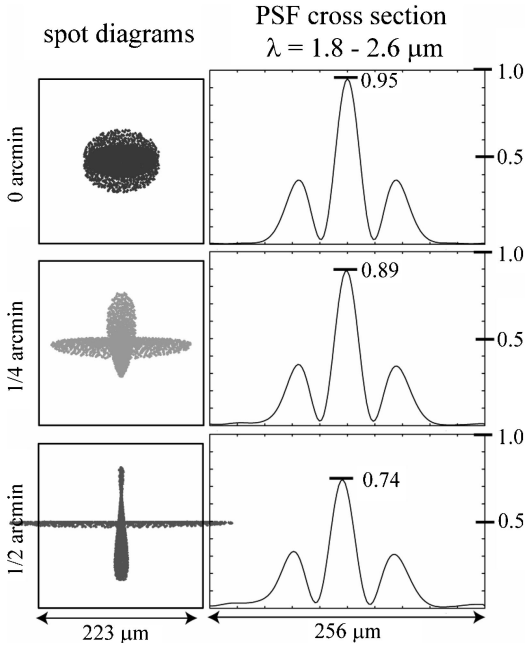

(b)

Fig. 11. Spot diagrams and cross sections of the PSFs (a) before and (b) after correction of linear piston errors in the LBT beam combiner. The PSFs were calculated for a rectangular spectrum of width 0.8 μm centered at 2.2 μm.

$$A(x,\,y) = \mathrm{Cyl}\left(\frac{1}{D}\sqrt{\left(x-\frac{\Delta}{2}\right)^2+y^2}\right) + \exp\left[i4\pi\cdot\frac{\xi}{D}\cdot\left(x-\frac{\Delta}{2}\right)\right] \times \mathrm{Cyl}\left(\frac{1}{D}\sqrt{\left(x+\frac{\Delta}{2}\right)^2+y^2}\right) \qquad (10)$$

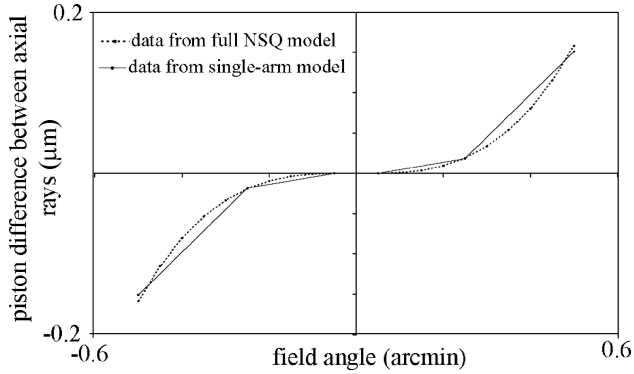

Fig. 12. Both single- and dual-arm models of the system show that the linear piston has been corrected and only higher-order piston errors remain in the LBT beam combiner.

where ξ is the displacement distance in waves at the edge of the tilted aperture, so that $\xi = (D/\lambda)\tan\alpha$ if α is a physical tilt on a primary. The resulting image intensity is

$$I(x,\,y) = \left(\frac{\pi D^2}{4\lambda f}\right)^2\left[\mathrm{Somb}^2\left(\frac{D}{\lambda f}r\right) + \mathrm{Somb}^2\left(\frac{D}{\lambda f}\sqrt{\left(x-\frac{2\xi}{D}\right)^2+y^2}\right) + 2\mathrm{Somb}\left(\frac{D}{\lambda f}r\right)\mathrm{Somb}\left(\frac{D}{\lambda f}\sqrt{\left(x-\frac{2\xi}{D}\right)^2+y^2}\right) \times\cos\left(2\pi\Delta\left(\frac{x}{\lambda f}-\frac{\xi}{D}\right)\right)\right]. \qquad (11)$$

As expected, one of the images shifts relative to the other. The center of the cosine fringes shifts as well, because the tilt in the aperture means that the two chief rays have equal OPLs at a different field angle and location on the image plane when compared to the system with no tilt error.

B. Evaluating Tilt Errors in a Ray-Trace Model

Tilt errors can be estimated by again tracing chief rays for each of the arms of the system. The coordinates of the chief ray in the image plane give an estimate of the image locations and thus the lateral image shifts. Image positions can be converted to tilt by using simple geometry:

$$W_{\mathrm{tilt}} = (1/\lambda)(D/2)(\Delta y/f), \qquad (12)$$

where W_{tilt} is the waves of tilt at the edge of the aperture, λ is the wavelength, D is the aperture diameter, Δy is the lateral image separation, and f is the focal length of the arm of the beam combiner. This information can be added to the piston information to reconstruct wave fans such as the one in Fig. 4 by using only sequential models of each arm of the system.

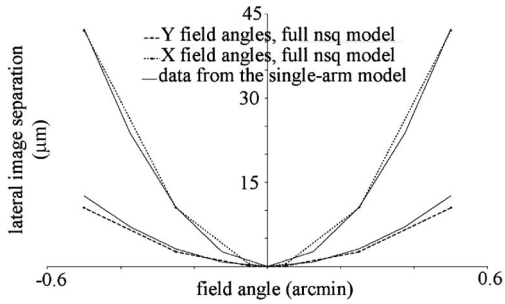

Fig. 13. Constant and linear image separations have been corrected in the LBT beam combiner. Quadratic image separations remain but do not dominate the system performance.

C. Eliminating Constant Tilt Errors by Matching On-Axis Image Locations

A tilt error that is constant as a function of field angle is just a pointing error in one of the arms of the interferometer. In a ray-trace program, the chief rays at zero field angle will not arrive at the same point in the image plane.

D. Eliminating Linear Tilt Errors by Matching Equal Focal Lengths

A tilt error that is a linear function of field angle indicates that the focal lengths of the arms of the interferometers are not equal. A trace of the chief rays versus field angle will show the presence of both linear and higher-order tilts as the chief rays separate in the image plane. If the focal lengths are properly matched, a plot of the separation versus field angle will not have a linear component.

E. Eliminating Quadratic Tilt Errors by Zeroing or Matching Distortions

Tilt errors that are quadratic as a function of field angle are due to mismatched distortions between the arms of the interferometer. The distortions can either be matched or driven to zero using traditional design techniques for controlling distortion. A plot of separation of the chief rays in the image plane versus field angle will show the presence of quadratic tilt errors.

F. Tilt Errors in the Large Binocular Telescope Beam Combiner

Constant and linear tilt errors have been eliminated in the LBT beam combiner because the focal lengths match (since the two arms are identical but flipped about the horizontal axis as shown in Fig. 1), and the arms have been positioned so that the on-axis images are coincident.

Quadratic tilt errors due to distortion differences remain in the beam combiner, as shown in Fig. 13. Since each arm in the LBT is not itself rotationally symmetric, the distortion pattern is also not symmetric and is skewed in one direction. Since the two LBT arms are identical but flipped about the horizontal axis, the distortion patterns from the two arms are skewed in opposite directions, causing the images to separate quadratically as a function of field angle. Since the system is dominated by astigmatism over the desired field of view, there is no need to correct the quadratic image separations.

5. Defocus Errors Cause Longitudinal Image Separation

A. Effect of Defocus on the Perfect Image

A defocus error in one of the apertures causes separation of the individual images into or out of the image plane (longitudinal image shift error). The entrance pupil amplitude can be expressed as

$$A(x,\ y) = \mathrm{Cyl}\left(\frac{1}{D}\left[\left(x-\frac{\Delta}{2}\right)^2+y^2\right]^{1/2}\right) + \exp\left\{i2\pi\beta\,\frac{4}{D^2}\left[\left(x-\frac{\Delta}{2}\right)^2+y^2\right]\right\} \times \mathrm{Cyl}\left(\frac{1}{D}\left[\left(x+\frac{\Delta}{2}\right)^2+y^2\right]^{1/2}\right). \quad (13)$$

In the extreme, the defocused aperture gives a broadened image that just contributes a constant intensity over the image plane and contributes nothing to the PSF height.

B. Evaluating Defocus Errors in a Ray-Trace Model

A single-arm model can be used to estimate defocus errors for reconstructed wave fans. The image locations as a function of field angle can be estimated by finding where the marginal and chief rays cross as a function of field angle for each arm in the system. The effect on a wave fan like the one in Fig. 4 can be calculated by using

$$\delta z/\lambda = -8\ (f\text{-number})^2\ W_{020}, \quad (14)$$

where δz is the defocus distance and W_{020} represents the waves of aberration at the edge of the aperture.[23]

C. Eliminating Constant Defocus Errors

Constant defocus errors mean that the intersection of marginal and chief rays will occur somewhere other than the image plane at zero field angle for one or both arms of the system. The image plane location may need to be adjusted, or a shift of the defocused arm or an adjustment of its power can be used to correct the error.

D. Eliminating Linear Defocus Errors by Correcting the Image Plane Tilt

Linear defocus errors are caused by an image plane that is tilted with respect to the location of the true image. A plot of the chief and marginal ray intersection versus the location of the image surface will show a linear component. If each arm of the interferometer has its own image plane tilt, the tilt of the image plane may need to be forced to zero during the design process.

The angle of the true image can be estimated by using the Scheimpflug condition[23] (well known to us-

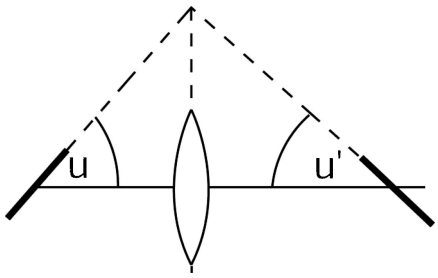

Fig. 14. Scheimpflug condition states that the object and image planes must intersect in the system's principal planes.

ers of large-format photographic cameras), which states that the object and image planes must intersect in a system's principal planes (see Fig. 14). This can be calculated analytically, but in a ray-trace program one can simply trace a ray that lies on the object surface. That ray must also lie on the surface of the image plane.

E. Eliminating Quadratic Defocus Errors by Matching or Zeroing Field Curvature

If a plot of the longitudinal image separation shows a quadratic component, then the field curvatures between the two arms differ. If a curved focal plane is tolerable, the field curvatures can be forced to be equal during the design process. If not, the field curvature must be forced to zero in the usual ways while designing an arm of the interferometer.

F. Defocus Errors in the Large Binocular Telescope Beam Combiner

The geometry of one arm of the LBT beam combiner shows that the image plane will be tilted. When the two arms are combined as shown in Fig. 1, the image planes will have equal but opposite tilts. The axial image separation that results is shown in Fig. 15. It is not necessary to correct this error, because astigmatism currently limits the system's field of view.

6. Aberrations in the Individual Images

The height of the combined PSF will also be degraded if other higher-order aberrations are present in any of the arms of the interferometer. Aberrations such as spherical, coma, and astigmatism can only reduce the PSF height. Matching the amounts of these aberrations in each arm will not give any improvement in the imaging. This is not the case for distortions and field curvatures, which do not degrade the height of the PSF.

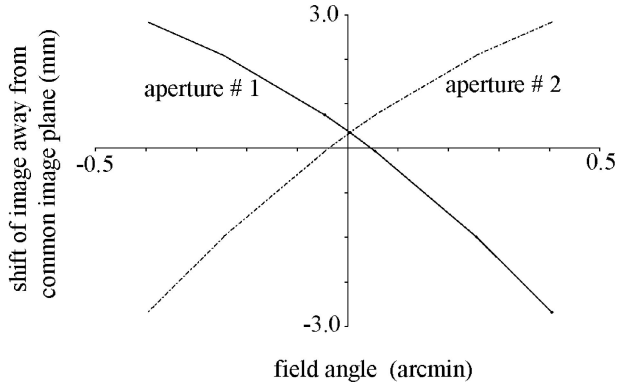

Fig. 15. Linear defocus errors remain in the LBT beam combiner but do not dominate the system's performance.

7. Summary

The low-order beam-combining errors discussed above dominate the performance of multiple-aperture systems over small field angles. The perfect image from a two-aperture system has three parts: an image from the first aperture, an image from the second aperture, and a set of fringes under the product of a Somb envelope and a coherence envelope. (For more than two apertures, the picture is similar; each aperture produces an image and each pair of apertures produces a set of interference fringes.) For perfect images over a wide field of view, all three of these elements must remain coincident in the image plane as a function of field angle. The images may not separate, the fringes may not shift away from the images, and the individual images cannot be aberrated.

Each of these errors can be corrected if the error is limiting the performance of the system. A summary of the correction methods for the low-order beam-combining errors is given in Table 1. All the low-order beam-combining errors are detectable in wave fans of the combined system. If the fringes shift, piston appears in wave fans of the system. If the images separate laterally, tilt appears between apertures in the wave fans. If the images separate longitudinally, defocus appears in the wave fans.

Piston that appears in the wave fans may not be significant if the piston is not a significant fraction of the coherence length of the system. One estimate of coherence length is $l_c = c/\Delta\nu$. Systems with smaller

Table 1. Correction Methods for Low-Order Beam-Combining Errors

Error, Effect	Correction
PISTON, fringe shift or reduction in coherence	
Constant piston errors	Match axial path lengths
Linear piston errors	Satisfy the sine condition for chief rays at a small field angle by using $h/(\sin u') = \Delta y/\alpha$
TILT, images separate laterally in the image plane	
Constant tilt errors	Set correct pointing in all telescope arms
Linear tilt errors	Match focal lengths in all arms
Quadratic tilt errors	Match or zero the distortion in all arms
DEFOCUS, images separate longitudinally in the image plane	
Constant defocus errors	Shift the image plane or set correct powers or shifts in each arm
Linear defocus errors	Match the tilt of the image surfaces for each arm
Quadratic defocus errors	Match or zero the field curvature of each arm

bandwidths can tolerate larger amounts of piston error.

Nonsequential models of multiple-aperture systems can be difficult to create and optimize in current ray-trace codes. It is preferable to design each arm of the interferometer separately in sequential mode, correcting for the low-order beam-combining errors during the design process. It is straightforward to predict the combined system's performance by tracing rays in each arm of the system and reconstructing what the combined wave fans will look like.

The piston in the wave fans can be calculated by finding the optical path lengths of the chief rays in the system. One aperture must be chosen as the reference aperture and will have the pathlength $\mathrm{OPL}_{\mathrm{ref}}$. Then the piston that appears on the other apertures in the wave fans will be $W_{\mathrm{piston}} = (\mathrm{OPL}_i - \mathrm{OPL}_{\mathrm{ref}})/\lambda$. The lateral image separation can be calculated by finding the image plane coordinates of the chief rays over the field of view of interest. If the distance between any two images is Δy, then the contribution to the wave fans from lateral image separation is $W_{\mathrm{tilt}} = (1/\lambda)(D/2)(\Delta y/f)$. Longitudinal image separation can be calculated by finding the coordinates of the intersection of the chief and the marginal rays with respect to the image plane. For an image separation of δz, the contribution to the wave fan can be found using $\delta z/\lambda = -8\,(f\text{-number})^2\,W_{\mathrm{power}}$.

References

1. J. E. Harvey and R. A. Rockwell, "Performance characteristics of phased array and thinned-aperture optical telescopes," Opt. Eng. **27,** 762–768 (1988).
2. R. V. Shack, J. D. Rancout, and H. Morrow, "Effects of dilution on a six-element synthetic aperture," Appl. Opt. **10,** 257–259 (1971).
3. M. J. E. Golay, "Point arrays having compact, nonredundant autocorrelations," J. Opt. Soc. Am. **61,** 272–273 (1971).
4. T. J. Cornwell, "A novel principle for optimization of the instantaneous Fourier plane coverage of correlation arrays," IEEE Trans. Antennas Propag. **36,** 1165–1167 (1988).
5. A. B. Meinel, "Aperture synthesis using independent telescopes," Appl. Opt. **9,** 2501–2504 (1970).
6. W. A. Traub, "Combining beams from separated telescopes," Appl. Opt. **25,** 528–532 (1986).
7. R. R. Butts, "Effects of piston and tilt errors on the performance of multiple mirror telescopes," in *Wavefront Distortions in Power Optics,* C. A. Klein, ed., Proc. SPIE **293,** 85–89 (1981).
8. R. V. Shack, "Aberration limitations on optical array telescopes," J. Opt. Soc. Am. **68,** 1361 (1978).
9. R. L. Lucke, "Influence of seidel distortion on combining beams from a phased telescope array," Appl. Opt. **38,** 4776–4783 (1999).
10. R. D. Sigler and A. L. Palmer, "Increasing the phased field of view of large distributed aperture telescope arrays," in *Current Developments in Lens Design and Optical Engineering II,* R. E. Fischer, B. Johnson, and W. Smith, eds., Proc. SPIE **4441,** 60–71 (2001).
11. J. E. Harvey, A. B. Wissinger, and A. N. Bunner, "A parametric study of various synthetic aperture telescope configurations for coherent imaging applications," in *Infrared, Adaptive and Synthetic Aperture Optical Systems,* R. B. Johnson, ed., Proc. SPIE **643,** 194–207 (1986).
12. J. E. Harvey and C. Ftaclas, "Field of view limitations of phased telescope arrays," Appl. Opt. **34,** 5787–5798 (1995).
13. L. D. Weaver, J. S. Fender, and C. R. DeHainaut, "Design considerations for multiple telescope imaging arrays," Opt. Eng. **27,** 730–735 (1988).
14. J. S. Fender, "Phased array optical systems," in *Infrared, Adaptive, and Synthetic Aperture Optical Systems,* R. B. Johnson, ed., Proc. SPIE **643,** 122–128 (1986).
15. N. V. Ryabova and D. N. Eskov, Multiaperture synthesis telescope systems with direct image formation," Sov. J. Opt. Technol. **60,** 507–521 (1993).
16. C. R. DeHainault, K. P. Henta, L. D. Waver, and J. D. Gonglewski, "Design of a wide field of view phased array telescope," Opt. Eng. **27,** 762–768 (1988).
17. E. Hege, J. Beckers, P. Strittmatter, and D. McCarthy, "Multiple mirror telescope as a phased array telescope," Appl. Opt. **24,** 2565–2576 (1985).
18. P. Salinari, "The Large Binocular Telescope," in *18th Congress of the International Comission for Optics,* A. J. Glass, J. W. Goodman, A. H. Guenther, and T. Asakura, eds., Proc. SPIE, **3749,** 691–692 (1999).
19. J. Gaskill, *Linear Systems, Fourier Transforms, and Optics* (Wiley 1978), see especially pp. 72, 200, 328–329.
20. R. Kingslake, *Lens Design Fundamentals* (Academic, 1978).
21. A. B. Meinel, "Aperture synthesis using independent telescopes," Appl. Opt. **9,** 2501–2504 (1970).
22. J. C. Wyant and K. Creath, "Basic wavefront aberration theory for optical metrology," in *Applied Optics and Optical Engineering,* R. Kingslake, ed. (Academic, 1992), Vol. 11.
23. H. M. Merklinger, "Scheimpflug's patent," *in Photo Techniques,* November–December 1996.